Research on the applicability of high-precision underground exploration technology to public roads in Bangkok: Part 2 – Risk assessment of cavities beneath concrete pavement

Chana Phutthananon[1] Warat Kongkitkul[2,*] Amara Cheamsuphakit[3] Warakorn Seedown[4] Hirunya Silakub[5]
Mitsumasa Yamashina[6] Jun Shinohara[7] and Naoki Kinoshita[8]

[1,2,3,4,5] *Department of Civil Engineering, Faculty of Engineering, King Mongkut's University of Technology Thonburi, Bangkok, THAILAND*
[6,7] *Center for Disaster Management Informatics Research, Ehime University, Matsuyama, JAPAN*
[8] *Department of Civil and Environmental Engineering, Ehime University, Matsuyama, JAPAN*
**Corresponding author; E-mail address: warat.kon@kmutt.ac.th*

Abstract

Detection and assessment of underground cavities have become critical in Thailand due to increasing sinkhole-related incidents. In Japan, cavity risks under asphalt pavement are classified into three categories: urgent, monitoring, and no action required, based on cavity depth and size, with detection enabled by advanced Ground Penetrating Radar Mobile Mapping System 3D (GMS3) technology. However, applying this risk classification to concrete pavement in Bangkok is complex due to differing soil and structural conditions. This study employs a two-dimensional finite element method to evaluate typical concrete pavement structures in Bangkok under varying cavity depth and size conditions. The results, categorized by slab responses, were validated through 1-g scaled-down model tests that physically simulated cavities and monitored soil and pavement responses. These findings aim to improve asset management reliability and inform effective maintenance strategies for Thailand's road infrastructure.

Keywords: Ground penetrating radar, Cavity, Finite element method, Physical model test, Risk evaluation

1. Introduction

The Ground Penetrating Radar Mobile Mapping System 3D (GMS3), developed by Canaan Geo Research Co., Ltd. in 2015 and validated in collaboration with Ehime University since 2017, integrates high-resolution ground penetrating radar (GPR) and a 360-degree camera-based Mobile Mapping System (MMS). It enables accurate detection of underground cavities and has been used to survey approximately 10,000 km annually in Japan.

In Japan, where asphalt pavement is common, GMS3 has been used to classify sinkhole risks into three categories, Risk A (urgent), Risk B (under observation), and Risk C (low), based on the cavity width (short side) and ceiling depth (Fig. 1). [1, 2]. This approach has proven effective in prioritizing safety interventions. However, applying this model directly to Thailand is not straightforward due to differences in pavement types (concrete in Bangkok), soil characteristics, groundwater behavior, and construction practices.

Sinkholes have become a growing concern in Thailand, especially in urban areas like Chaeng Watthana Road, where eight incidents were reported between 2022 and 2025, caused by factors such as heavy rain, pipe leakage, and underground utility work. These events have prompted renewed efforts in cavity detection and prevention.

Studies in Japan indicate that sinkholes often stem from underground pipe leaks, where groundwater infiltration leads to soil erosion, forming voids that compromise structural stability [3, 4]. In Thailand, similar processes are further complicated by extensive underground construction, which can disturb soil and initiate void formation. Sinkholes typically emerge when voids reach a critical size, and the overlying ground can no longer support surface loads, resulting in sudden collapse (Fig. 2) [5, 6]. This process can be accelerated by water infiltration, making understanding of these mechanisms vital for effective risk mitigation.

Although GMS3 can identify cavity locations, diameters (D) or the short-side widths, and crown (or ceiling) depths (H_c), existing Japanese risk assessment charts are not directly applicable to Bangkok's concrete pavement and subsoil conditions. Moreover,

limited research exists on how variations of D and H_c parameters influence sinkhole formation, especially for concrete pavements, with almost no experimental studies available.

This study addresses that gap by conducting: (1) physical model tests simulating concrete pavement over cavities at various D and H_c values, and (2) two-dimensional (2D) finite element (FE) analyses of concrete pavement under Bangkok subsoil conditions, using the same cavity configurations.

The development of cavities was simulated both physically and numerically by reducing soil volume, with pavement bending strain used as an indicator of sinkhole risk. The results demonstrated that bending strain increases with volume loss (VL), and that strain contours can potentially define risk zones based on cavity diameter (D) and crown depth (H_c). While the findings offer initial insight into the relationship between cavity characteristics and pavement response, only a limited series of FEM simulations and a single physical test case have been completed. Therefore, a full risk assessment chart specific to Bangkok has not yet been proposed. This study serves as a conceptual foundation, highlighting the potential for localized risk chart development, and underscores the need for further experimental and numerical investigation to support comprehensive implementation.

2. Methodology

2.1 Typical concrete pavement structure in Bangkok

The typical structure of concrete pavement (Fig. 3) is based on the standard drawing from the Bangkok Metropolitan Authority (BMA). From top to bottom, the structure comprises a 0.20 m thick concrete slab, a 0.25 m thick subbase, a 0.30-m-thick sand embankment layer, and an earth embankment with variable thickness depending on the required fill height.

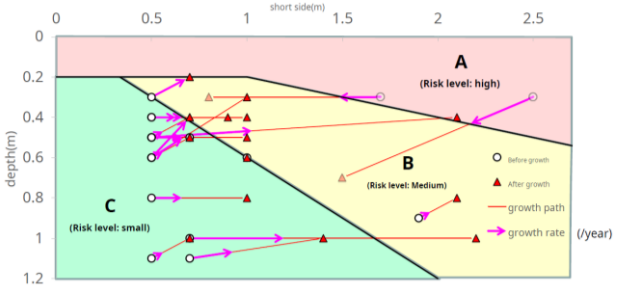

Fig. 1 An evaluation sheet for underground cavities adopted by the Japanese Ministry of Land, Infrastructure, Transport and Tourism and data plotting the process of cavity growth [1].

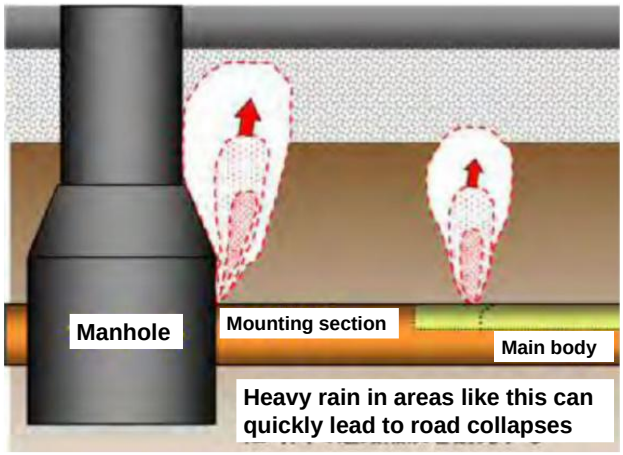

Fig. 2 Void formation caused by damaged sewer pipes [6].

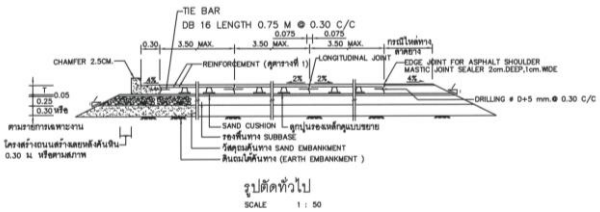

Fig. 3 Typical concrete pavement structure in Bangkok.

2.2 Physical model test

2.2.1 Modeling of concrete pavement structure

A scaled-down physical model of the concrete pavement structure was constructed in a sand box measuring 180 cm in length, 40 cm in width (out-of-plane), and 80 cm in depth (Fig. 4). The left, right, and bottom sides were reinforced with steel frames, while the front and rear sides were made of large acrylic panels to allow visual observation and for photogrammetric analysis.

The prototype pavement, consisting of a 20-cm-thick concrete slab (see Fig. 3), has elastic properties, Young's modulus (E), moment of inertia (I), and flexural stiffness (EI), as listed in Table 1. For the model, the slab was scaled down by a factor of 10 using a 6-mm-thick aluminum plate, with corresponding E, I, and EI values, as also listed in Table 1. The comparison between target and achieved scaling factors is provided.

While the achieved scaling factor for EI was 10.71, very close to the target of 10, the scaling factor for thickness was 33.33, which deviates significantly. However, since EI is the dominant parameter governing structural similarity in this pavement problem, the chosen model is considered acceptable.

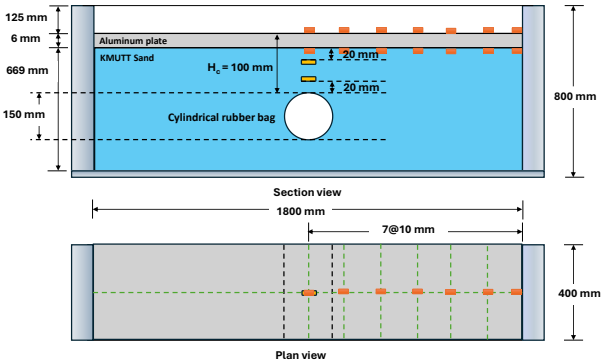

Fig. 4 Schematic section and plan views of the scaled-down physical model of a concrete pavement structure.

Table 1 Comparison of dimensional and mechanical properties between the prototype and scaled-down concrete pavement model.

Characteristics	Prototype reinforced concrete	Aluminum plate model	Target scaling factor	Achieved scaling factor
Width, *b* (cm)	40	40	1	1
Thickness, *h* (cm)	20	0.60	10	33.33
Young's modulus, *E* (GPa)	24.87	70	-	-
Moment of inertia, *I* (m^4)	$2.67x10^{-4}$	$7.20x10^{-9}$	-	-
Flexural stiffness, *EI* ($N-m^2$)	$6.63x10^{-6}$	$5.04x10^{-2}$	10^4	10.71^4

2.2.2 Modeling of pavement substructure materials

Replicating all individual layers beneath the concrete pavement as shown in Fig. 3 using different materials in the physical model is highly complex. Literature suggests that these layers can be effectively represented by a single equivalent material. Additionally, accurately modeling the weathered crust and very soft Bangkok clay requires reconstituting remolded clay, which is time-consuming and limits the number of test cases that can be performed within a given timeframe.

In this study, the substructure materials below the concrete slab, namely, sand cushion, subbase, and sand embankment, were modeled using KMUTT sand. Given the cohesive nature of clay, voids in clay layers are less likely to evolve into sinkholes. Moreover, in many real-world scenarios in Bangkok, sand embankments are significantly thick to raise pavement elevations. Based on these assumptions, KMUTT sand was selected as the representative material.

KMUTT sand is a sub-angular riverbed sand sourced from Thailand. It is prepared by flushing with tap water to remove impurities, oven-drying, and sieving to pass through a No. 40 sieve while being retained on a No. 100 sieve. This sand has been widely used in geotechnical experiments at King Mongkut's University of Technology Thonburi (KMUTT) [7-10].

2.2.3 Cavity modeling

In this study, a custom-designed cylindrical balloon (Fig. 5a) was used to simulate cavities by enabling gradual volume loss within a KMUTT sand medium [11]. The balloon, made of flexible rubber, measures 15 cm in diameter and 37.6 cm in length. It contains an internal cylindrical sponge that fits snugly inside, with stiffness selected to match that of KMUTT sand under corresponding overburden pressure at the intended installation depth.

Before use, the balloon is fully saturated by flushing it with de-aired water through the water circuit shown in Fig. 5b. KMUTT sand was placed in the test box using the air-pluviation method, known for ensuring uniformity and controlled density. After saturating and sealing the balloon, it was placed at the designated H_c along the centerline of the physical model. Additional KMUTT sand was then pluviated to fill the box to the top, followed by surface leveling and placement of the aluminum plate.

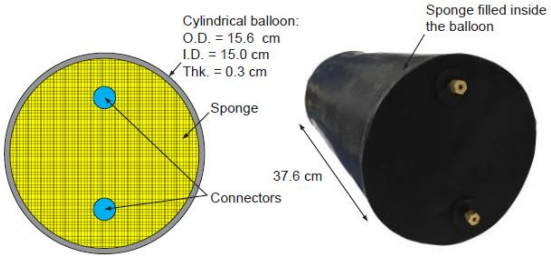

(a)

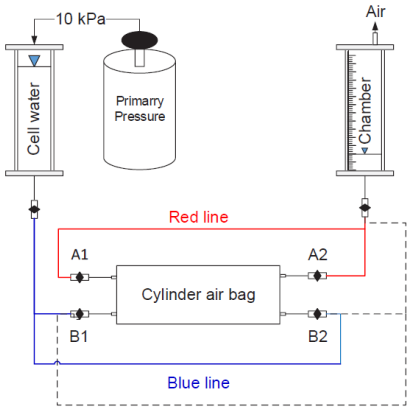

(b)

Fig. 5 Details of volume loss simulation: (a) cylindrical balloon used to simulate volume loss beneath the pavement structure; and (b) drainage system connected to the balloon for controlled volume reduction [11].

Table 2 Combinations of H_c and D investigated in this study.

Series	H_c (mm)	D (mm)
A	190	150
B	250	150
C	310	150

This study focuses on three different D and H_c values, as listed in Table 2. These values represent typical dimensions observed in the field that have the potential to develop into sinkholes. However, at the time of manuscript preparation, only a 15 cm in diameter balloon was available, and testing has been completed for the case with H_c = 19 cm.

2.2.4 Instrumentation and loading in the physical model

Various strain gauges were installed on the top and bottom sides of the aluminum plate used to model the concrete pavement at seven different distances from the centerline (Fig. 4). Two strain gauges were attached for the same distance, one on top and the other on bottom. Each strain gauge couple was connected in the form of an adjacent two-active two-dummy Wheatstone bridge for bending strain measurement. In addition, two earth pressure transducers (EPT) were installed inside the KMUTT sand layer at the centerline (Fig. 4). In this study, traffic loading was modeled with static surcharge, which is 2000 kg/m², and with n = 10, it becomes 200 kg/m² for the physical model. For the entire area of the aluminum plate of 1.8 × 0.4 m, it requires a total surcharge mass of 144 kg. In this study, ten sandbags specially designed to fit the sand box, each having a mass of 14.4 kg, were used to provide the surcharge (Fig. 6). Furthermore, the settlement of the aluminum plate was measured at the centerline and at two different distances from the centerline as shown in Fig. 6. During a test, photos were taken for subsequent photogrammetric analysis to observe the shear strain mobilized in the sand layer.

2.2.5 Test procedures

In this study, cylindrical balloons with an inner diameter of 15 cm were placed at H_c of 19 cm within the KMUTT sand layer to simulate underground cavities. To replicate VL, the water inside each balloon was gradually drained, causing the balloon to shrink and thereby mimicking the formation of a void beneath the pavement.

During the simulation, several responses were continuously monitored. These included bending strains and settlements of

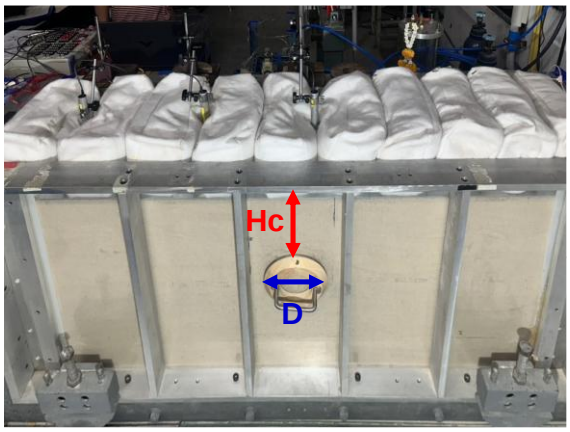

Fig. 6 Installation of sandbags to simulate surcharge loading and displacement transducers to measure pavement settlement.

the aluminum plate (representing the concrete pavement), earth pressure at selected depths, and soil deformation within the surrounding sand layer. The data collected from these measurements were used to develop relationships between the pavement responses and the extent of VL. These relationships form the basis for assessing the likelihood of sinkhole development under different cavity conditions.

2.3 Finite element method

This study employs FE analysis using the PLAXIS 2D software to simulate cavity development by gradually increasing VL, representing the subsidence of a sinkhole. The objective is to analyze strain beneath the center of a concrete pavement, which serves as a risk indicator for assessing potential hazards. The analysis considers various D and H_c of the cavity to provide early warning and mitigation strategies.

The FE analysis is categorized into three series with different H_c values of 1.0, 1.5, and 2.0 m based on the detection capability of GPR, which can identify effectively underground cavities at depths of approximately from 0.5 to 3.0 m. In each H_c, three are three D values of 1.5, 2.0, and 2.5 m.

2.3.1 Finite element geometry and modeling

The FE modeling was developed using real-scale dimensions without scaling down. Figs. 7(a) and 7(b) illustrate the boundary conditions and FE mesh used in the current study, respectively. In this study, soil and concrete pavement are represented using a 15-noded triangular plane strain element.

Based on the previous study [12], the optimal model dimensions for simulating a sinkhole using 2D FE model should have a horizontal length of at least 5H_c m from the center of FE

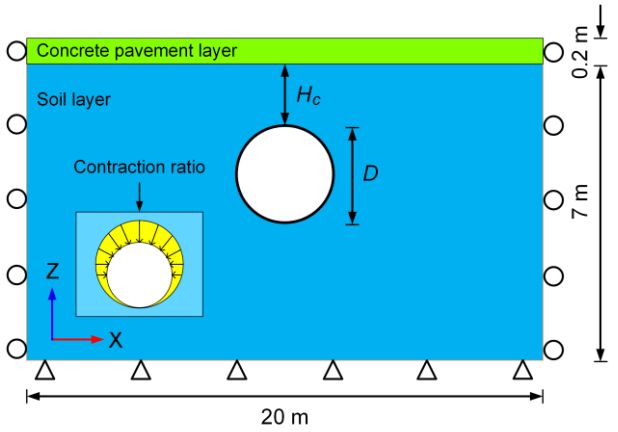

(a)

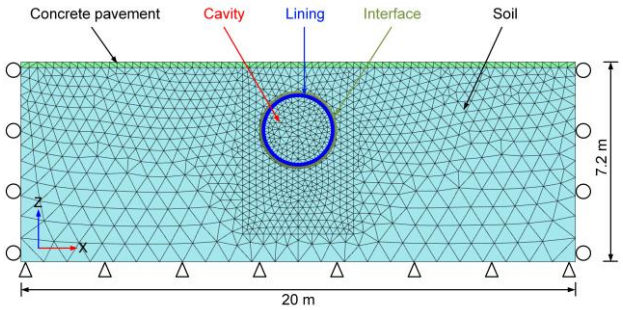

(b)

Fig. 7 2D numerical modeling used for this study: (a) FE geometry and (b) FE mesh.

Table 3 Material parameters of soil and concrete pavement used for FE analysis [13, 14].

Parameters	Soil	Concrete pavement
Soil model	Mohr-Coulomb	Linear Elastic
Drained type	Drained	Non-porous
Unsaturated unit weight (kN/m^3)	16.5	25
Saturated unit weight (kN/m^3)	20	-
Young's modulus (kPa)	80,000	8x10^6
Poisson's ratio (-)	0.3	0.2
Effective cohesion (kPa)	11	-
Effective friction angle (deg.)	31	-

Table 4 Material parameters for lining.

Parameters	Values
Axial stiffness, *EA* (kN/m)	300
Flexural stiffness, *EI* (N-m^2)	0.3
Lining thickness (m)	0.11

model and a depth extending at least 2 m from the bottom boundary of cavity. For this study, the model width (sand layer) is set to 20 m, which exceeds 5H_c in all cases. The model depth is assigned to 7 m in all investigated scenarios. The concrete pavement with a thickness of 0.2 m is placed on surface of sand layer, following the typical concrete pavement structure in Bangkok.

The bottom boundary of the FE model is fully constrained to prevent movement in all directions. The two vertical sides of the model are constrained only for horizontal movement. These boundary conditions are applied consistently across all FE cases of this study.

2.3.2 Material parameters

In this study, the Mohr-Coulomb model was used to simulate the behavior of soil, with the material model parameters used for the analysis presented in Table 3 [13, 14]. For the concrete pavement, the linear elastic model was applied to represent its behavior, as also shown in Table 3.

2.3.3 Finite element analysis procedure

The FE calculation was used to analyze sinkhole formation and study how pavement bending strain (horizontal strain in FE analysis) increases with VL of cavity increased. The cavity was simulated similarly to a tunneling simulation using the tunnel tool, with a lining modeled as a plate element. This approach allows for the control of VL by adjusting the contraction ratio (CR), with the relevant lining parameters provided in Table 4. The lining was assigned a thin cross-section relative to the cavity size, ensuring it remained the thinnest possible while maintaining computational feasibility. This design choice ensured that the lining properties did not influence the strain responses beneath the pavement. The FE simulation process consisted of three main steps, as outlined below:

First step - initial stress state simulation: the initial stress state of the soil mass (gravity loading) was established based on soil unit weight and the coefficient of earth pressure at rest.

Second step - concrete pavement modeling: a 0.2-m-thick concrete pavement was modeled on top of the soil layer to simulate actual field conditions.

Third step - sinkhole formation simulation: The cavity development was simulated by incrementally increasing CR in steps of 1% until failure occurred. The CR increments were then adjusted based on the rate of strain change beneath the concrete pavement. In regions where strain changed rapidly, smaller CR increments were successfully applied to capture the development of sinkhole formation more accurately. The

resulting critical strain point was used as a risk parameter to generate strain contours, which defined different risk zones.

3. Results and Discussions

3.1 Physical model test results

3.1.1 Maximum shear strain localization in sand

In the case of simulating damage of sinkhole formation on the pavement structure, VL of the rubber bag was simulated by draining the water from cylindrical balloon to the chamber. During this process, images were taken to analyze the strain field of soil, as shown in Fig. 8.

Figs. 8(a) and 8(b) show the maximum shear strain contours at volume loss (VL) levels of 5% and 10%, respectively. At VL = 5%, the failure in the supporting sand begins directly above the cavity, initiating deformation in the sand layer beneath the modeled pavement. At this stage, the formation of a cavity beneath the pavement is clearly observed. As VL increases to 10%, the failure zone expands, and the cavity beneath the pavement grows significantly larger. These results support the hypothesis that cavity development induced by volume loss is effectively captured by horizontal or bending strain responses in the pavement structure.

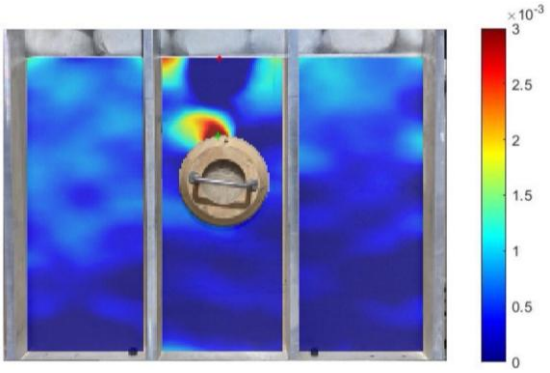

(a)

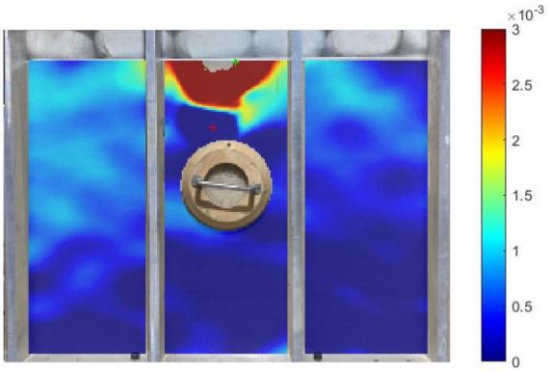

(b)

Fig. 8 Contour of maximum shear strain mobilized in sand at different VL values: (a) VL = 5%; and (b) VL = 10%.

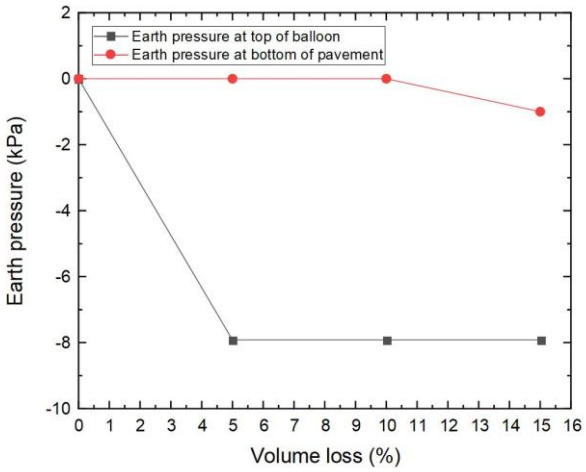

Fig. 9 Relationship between earth pressure and VL.

3.1.2 Earth pressure

In the scaled-down physical model test, earth pressure was measured to evaluate the impact of increasing soil VL on subsurface stress distribution. EPTs were installed at two key locations: above the balloon and beneath the pavement, to record changes in earth pressure as the VL incrementally increased to 5%, 10%, and 15%.

The experimental results (Fig. 9) demonstrate that earth pressure gradually decreases with increasing volume loss (VL), primarily due to the formation and expansion of the underground cavity, which alters the stress distribution within the soil mass. The most significant pressure reduction occurs near the center of the cavity, where the supporting soil weakens as VL progresses. This trend is clearly shown in the relationship between earth pressure and VL in Fig. 9. As the cavity enlarges, the reduction in soil stress becomes more pronounced, particularly directly above the cavity. These observations indicate the development of a soil arching effect, where stresses are progressively redistributed to the surrounding soil as the cavity expands.

3.1.3 Pavement settlement

According to the physical model test, the settlement of the pavement was measured using displacement transducers (DTs) under conditions of incremental soil VL, increasing sequentially to 5%, 10%, and 15%. A constant load of 144 kg, equivalent to the 20 kPa surcharge in the prototype, was applied to the modeled pavement.

The settlement recorded by the DTs at various measurement points increased with higher VL. As seen in Fig. 10, the central position exhibited the highest settlement, consistent with the concept that areas closer to the center of the underground cavity

are more affected by VL. In contrast, settlement values decreased progressively at positions located 35 cm and 70 cm away from the center to the left. These correspond to 3.5 meters and 7 meters in the prototype, respectively.

3.1.4 Bending pavement strain

In this study, the pavement bending strains were measured using strain gauges to evaluate the behavior of the pavement under varying VL conditions.

The results indicate that pavement bending strain is directly related to VL. As the VL increases, the measured pavement bending strain changes accordingly. The increase in VL leads to an uneven distribution of stress across the pavement, resulting in increased pavement bending strain at certain locations.

Fig. 11 clearly demonstrates that when VL increases from 5% to 10% and 15%, the pavement bending strain at the central position of the pavement increases significantly, highlighting its sensitivity to the stress induced by soil volume reduction in areas directly affecting pavement stability.

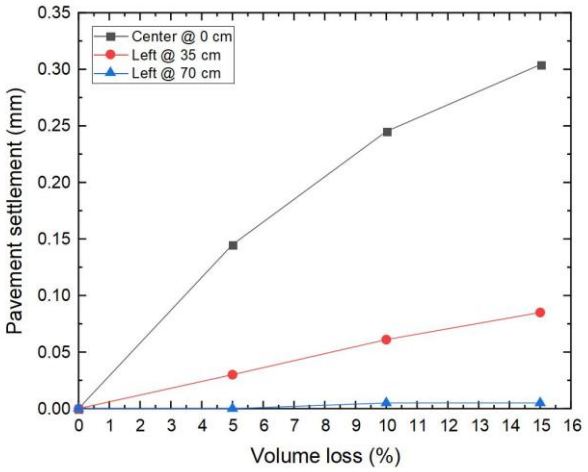

Fig. 10 Relationship between pavement settlement and VL.

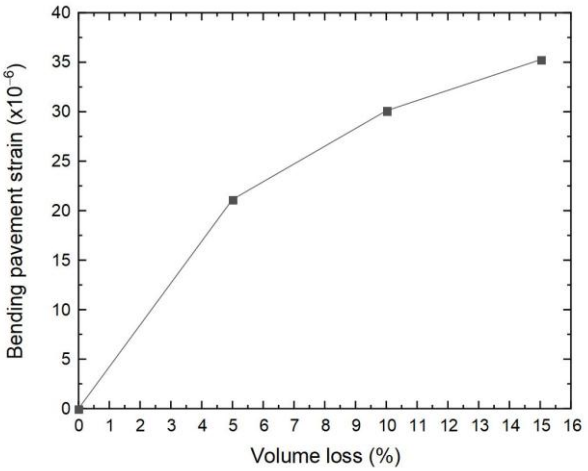

Fig. 11 Relationship between pavement bending strain (horizontal strain underneath the pavement) and VL.

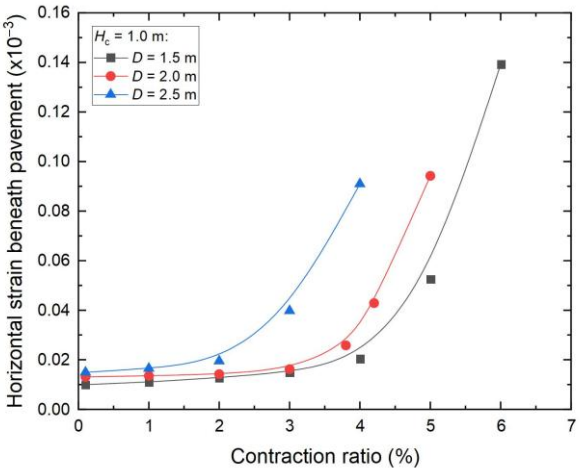

Fig. 12 Relationship between horizontal strain beneath pavement and CR for case of H_c = 1.0 m.

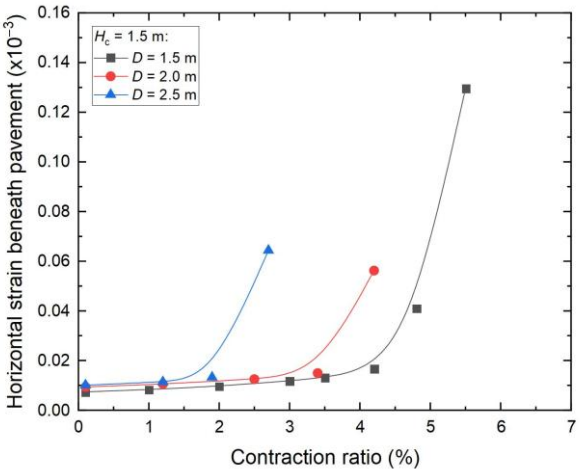

Fig. 13 Relationship between horizontal strain beneath pavement and CR for case of H_c = 1.5 m.

3.2 Finite element analysis results

3.2.1 Relationship between horizontal strain and CR

At H_c = 1.0 m (Fig. 12), horizontal strain beneath pavement displays a non-linear relationship with CR variation, remaining low (below 0.02×10^{-3}) until CR = 2% before increasing rapidly, especially beyond CR = 3%. The different *D* values show distinct behaviors: *D* = 1.5 m maintains the lowest strain until CR of 5% before dramatically rising to 0.14×10^{-3} at CR of 6%; *D* = 2.0 m shows intermediate values reaching 0.095×10^{-3} at CR = 5%; and *D* = 2.5 m exhibits the highest strain values, reaching 0.09×10^{-3} at

just CR of 4%. When H_c increases to 1.5 m (Fig. 13), similar patterns emerge with strain remaining low until CR = 2%, though divergence between D values occurs earlier than with H_c = 1.0 m.

As H_c increases to 2.0 m (Fig. 14), a substantial reduction in overall strain magnitude is observed, with maximum values reaching only 0.04×10^{-3} compared to 0.16×10^{-3} in previous scenarios. D = 1.5 m shows gradual increase strain to a maximum of 0.021×10^{-3} at CR = 5%; D = 2.0 m reaches 0.019×10^{-3} at CR of 4.5%; while D = 2.5 m data extend only to 2.5% CR, reaching 0.014×10^{-3}. These results indicate that increasing H_c significantly reduces pavement strain across all investigated scenarios, while the influence of D value creates distinct strain development patterns at different CR values.

3.2.2 Discussion on FE results

The relationship between horizontal strain and CR is profoundly influenced by both H_c and D parameters. As H_c increases from 1.0 m to 2.0 m, the pavement demonstrates substantially improved resistance to horizontal strain development, suggesting that cavity located deeper provides enhanced structural stability. For any given H_c value, larger D values generally result in earlier onset of significant strain, indicating that large cavity may experience accelerated strain development at lower CR thresholds. The data consistently shows critical contraction ratio thresholds between 2-4%, beyond which strain increases non-linearly, with this threshold decreasing as D increases. The dramatic reduction in strain magnitude when H_c increases highlights the paramount importance of this parameter in controlling strain development beneath pavement structures, which has significant implications for optimizing pavement design to enhance durability and performance under varying contraction conditions.

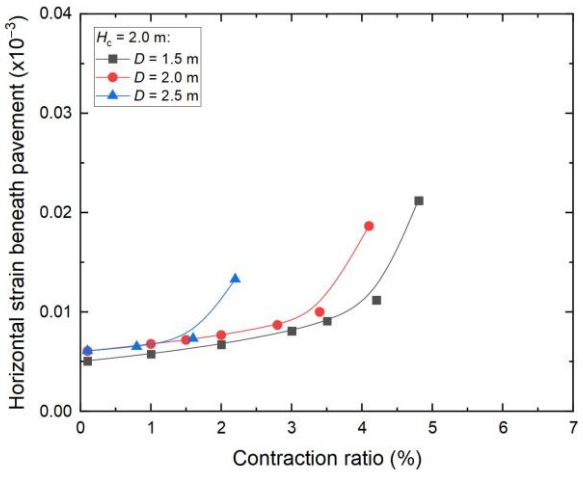

Fig. 14 Relationship between horizontal strain beneath pavement and CR for case of H_c = 2.0 m.

The analysis demonstrates that horizontal strain beneath pavement is significantly influenced by both the H_c and D parameters, as well as the contraction ratio. Increasing Hc from 1.0 m to 2.0 m provides substantial benefits in terms of strain reduction, while the impact of varying D values is more complex and depends on the CR.

4. Conclusions

This study explored the applicability of Japan's sinkhole risk classification framework to Bangkok's concrete pavement systems by combining scaled-down physical model tests and finite element (FE) simulations. The key findings are summarized as follows:

1. The scaled-down physical model tests demonstrated that pavement bending strain, surface settlement, and earth pressure respond sensitively to cavity volume loss (VL). As VL increased, strain localized above the cavity, central settlement intensified, and earth pressure decreased, supporting the use of pavement strain as a practical sinkhole risk indicator.
2. FE analysis showed that horizontal strain beneath the pavement increases non-linearly with the contraction ratio (CR), particularly beyond a threshold of 2–4%. Greater cavity depths (Hc) enhanced resistance to strain development, whereas larger diameters (D) accelerated strain onset at lower CR values.
3. The results highlight that direct application of Japan's sinkhole risk classification is unsuitable for Bangkok due to fundamental differences in pavement type, soil conditions, and construction practices. A localized assessment approach is necessary to account for Bangkok's unique geotechnical and structural context.

Although this research lays the groundwork for a Bangkok-specific risk assessment methodology, the authors acknowledge its limitations. The current findings are based on a single physical test case and a limited number of FE simulations with generalized input parameters. Further experimental and numerical studies are required to develop a robust and comprehensive risk classification framework for practical implementation.

Acknowledgement

The authors gratefully acknowledge the financial support provided by King Mongkut's University of Technology Thonburi (KMUTT), Thailand Science Research and Innovation (TSRI), and National Science, Research and Innovation Fund (NSRF) Fiscal year 2025 under the project Innovation and advanced technology for future construction with sustainability, Grant number (FRB680074/0164)

References

[1] Kuwano, R., Ohara, Y. and Sera, R. (2019). A study on the potential size of subsurface cavities in sandy soil. *16th Asian Regional Conference on Soil Mechanics and Geotechnical Engineering (16ARC)*, Taipei, Taiwan, pp. 1-7.

[2] Kuwano, R. (2011). Subsurface cavities and road cave-ins. *IPA News Latter*, 6, pp. 1-7

[3] Koike, Y., Sera, R. and Kuwano, R. (2012). Discussion on the occurrence of cavities under the road surface (Part 1). In *47th Annual Geotechnical Engineering Research Presentation*, Hachinohe, Japan.

[4] Shiau, J., Chudal, B. and Keawsawasvong, S. (2022). Three-dimensional sinkhole stability of spherical cavity. *Acta Geotechnica*, 17, pp. 3947-3958.

[5] Waltham, T., Bell, F.G. and Culshaw, M.G. (2005). *Sinkholes and subsidence: karst and cavernous rocks in engineering and construction*, Springer Science & Business Media.

[6] Japan International Cooperation Agency (JICA). (2016). Project feasibility study related to strengthening resilience: Japanese road cave-in risk diagnosis technology and the road network utilized, Geo Search Co., Ltd.

[7] Chantachot, T., Kongkitkul, W., Youwai, S. and Jongpradist, P. (2016). Behaviours of geosynthetic-reinforced asphalt pavements investigated by laboratory physical model tests on a pavement structure. *Transportation Geotechnics*, 8, pp. 103-118.

[8] Dararat, S., Warat, K., Goran, A. and Ling, H.I. (2021). Estimation of stress state-dependent elastic modulus of pavement structure materials using one-dimensional loading test. *Road Materials and Pavement Design*, 22, pp. 245-267.

[9] Punya-in, Y. and Kongkitkul, W. (2022). Effects of temperature on the stress-strain-time behavior of sand under shear. *Journal of Testing and Evaluation*, 51, pp. 686-705.

[10] Jariyatatsakorn, K., Kongkitkul, W. and Tatsuoka, F. (2024). Prediction of creep strain from stress relaxation of sand in shear. *Soils and Foundations*, 64, pp. 101472.

[11] Siripuksa, C. and Kongkitkul, W. (2020). Acceleration of pavement structure strains in a physical model with volume losses in subgrade. *Engineering Journal Chiang Mai University*, 27, pp. 62-78. (In Thai)

[12] Abbas, Q., Ali, T., Asad, A.T. and Aslam, M. (2024). Analyzing the impact of geosynthetic reinforcement on sinkhole: A numerical investigation with machine learning approach. *Engineering Failure Analysis*, 157, pp. 107915.

[13] Jongpradist, P., Kaewsri, T., Sawatparnich, A., Suwansawat, S., Youwai, S., Kongkitkul, W. and Sunitsakul, J. (2013). Development of tunneling influence zones for adjacent pile foundations by numerical analyses. *Tunnelling and Underground Space Technology*, 34, pp. 96-109.

[14] Rukdeechuai, T., Jongpradist, P., Wonglert, A., Kaewsri, T., 2009. Influence of soil models on numerical simulation of geotechnical works in Bangkok subsoil. *EIT Research and Development Journal*, 20, pp. 17–28.